Journal of Nuclear Materials 400 (2010) 46–55

Contents lists available at ScienceDirect

Journal of Nuclear Materials

journal homepage: www.elsevier.com/locate/jnucmat

Hardening and microstructural evolution in A533B steels under neutron irradiation and a direct comparison with electron irradiation

K. Fujii [a,*], H. Nakata [a], K. Fukuya [a], T. Ohkubo [b], K. Hono [b], Y. Nagai [c], M. Hasegawa [c], T. Yoshiie [d]

[a] Institute of Nuclear Safety System, Mihama-cho, Mikata-gun, Fukui 919-1205, Japan
[b] National Institute for Materials Science, Tsukuba, Ibaraki 305-0045, Japan
[c] Tohoku University, Oarai-cho, Higashi Ibaraki-gun, Ibaraki 311-1313, Japan
[d] Kyoto University, Kumatori-cho, Izuminami-gun, Osaka 590-0494, Japan

ARTICLE INFO

Article history:
Received 15 April 2008
Accepted 10 February 2010

ABSTRACT

A533B steels irradiated at 290 °C up to 10 mdpa in the Kyoto University Reactor were examined by hardness, positron annihilation and atom probe measurements. Dose dependent irradiation hardening and formation of Cu-rich clusters were confirmed in medium Cu (0.12% and 0.16%Cu) steels whereas neither hardening nor cluster formation was detected in low Cu (0.03%Cu) steel. No microvoids were formed in any of the steels. Post-irradiation annealing in medium Cu steels revealed that the hardening recovery at temperatures above 350–400 °C could be attributed to compositional changes and dissociation of the Cu-rich clusters. Compared to electron irradiation at almost the same dose and dose rate, KUR irradiation caused almost the same hardening and produced Cu-rich clusters, more solute-enriched with larger size and lower density. Considering lower production of freely-migrating vacancies in neutron irradiation, the results suggested that cascades enhance the formation of Cu-rich clusters.

1. Introduction

Radiation embrittlement of reactor vessel steels is one of the important degradation phenomena in the continued long-life safe operation of light water reactors (LWRs). To forecast the long-life integrity of vessel steels considering various material variables and irradiation conditions, it is necessary to use predictive models for embrittlement based on physical mechanisms [1–4]. This needs a sound understanding of the physical mechanisms of microstructural evolution during irradiation.

In the current framework of mechanisms of radiation embrittlement proposed by Odette and Lucas [5], Cu-rich precipitates or clusters are the main contributor to hardening-induced embrittlement in Cu-containing steels. Radiation-induced secondary defects other than Cu-rich clusters, so-called matrix damage, provide an additional contribution to embrittlement in high Cu steels and become a main contributor to embrittlement in low Cu steels. They also predicted that the Mn–Ni phase, often called the late blooming phase, is formed in low Cu high Ni steels at high doses. Recent studies using advanced microanalysis techniques such as three-dimensional atom probe and advanced positron annihilation provided additional knowledge of microstructural features [6]. The formation of Cu-free or very low Cu clusters consisting of Mn, Ni and Si atoms in very low Cu steels and interstitial dislocation loops has recently been confirmed [7–9]. The formation process and contribution to embrittlement of these features are not yet fully understood.

Solute clustering under irradiation is supposed to be dominated mainly by radiation-enhanced vacancy-driven diffusion and thermodynamic phase stability. In this context, the production rate of freely-migrating vacancies, which depends on the primary knock-on spectrum, is an essential parameter for microstructural evolution. It was demonstrated that the accumulated number of vacancy jumps has a direct relation to dose rate effects on microstructural evolution [10]. However, although it is well known that cascade damage directly produces clusters of vacancies or interstitials and provides a spatially inhomogeneous distribution of defects, the role of cascades is not well understood in low alloy steels. To elucidate the effects of cascades on microstructural evolution and hardening, comparisons of low-PKA-energy irradiation such as electron irradiation with high-PKA-energy irradiation such as fast neutron or heavy ion irradiation have been conducted. Some of such studies showed that electron irradiation has almost the same hardening efficiency as neutron irradiation on a dpa basis in model alloys and commercial steels [11–13], whereas the concentration of freely-migrating defects is much higher for electron irradiation [14,15]. Other studies pointed out an enhancement effect of cascade damage under neutron irradiation on Cu precipitation in Fe–Cu alloys compared to electron irradiation [16–18]. Some of the present authors examined hardening and microstructural evolution in medium Cu A533B steels after 5 MeV electron irradiation

* Corresponding author. Tel.: +81 770 37 9114; fax: +81 770 37 2009.
E-mail address: fujiik@inss.co.jp (K. Fujii).

0022-3115/$ - see front matter © 2010 Elsevier B.V. All rights reserved.
doi:10.1016/j.jnucmat.2010.02.008

to 22 mdpa and compared the data with higher dose neutron data [11]. They found almost the same hardening efficiency and evolution of Cu-rich clusters and pointed out the existence of cascade effects and direct formation of Cu-rich clusters from each cascade. However, these previous studies did not provide direct evidence in the strict sense since the dose and dose rate were much different between electron and neutron irradiation. A more direct comparison of microstructure and hardening would be useful for clarifying the cascade effects on solute clustering processes.

In the present study, hardening and microstructural evolution were examined in medium and low Cu A533B steels irradiated to 10 mdpa in the Kyoto University Reactor (KUR) at 290 °C. The irradiation was performed at almost the same dose and dose rate as the previous electron irradiation on the medium Cu steels. Post-irradiation annealing (PIA) experiments were also conducted for both KUR- and electron-irradiated medium Cu steels to investigate the stability of clusters and other features. This enables us to make a more direct and detailed comparison of hardening and microstructural evolution in medium Cu steels between electron and neutron irradiation.

2. Experimental procedures

2.1. Materials and irradiation

Two heats of medium Cu A533B plates (steel A with 0.12%Cu and steel B with 0.16%Cu), and one heat of low Cu A533B plate (steel C with 0.03%Cu) were used in this study. The chemical compositions are shown in Table 1. Disk shaped specimens measuring $\varnothing 5 \times t$ 0.3 mm and rod shaped specimens measuring $0.3 \times 0.3 \times 10$ mm were machined from blocks of the steels. The disk shaped specimens were mechanically polished using wet grinding on SiC papers down to 1200 grit and 3 μm diamond buff.

Neutron irradiation was carried out using the Materials Controlled Irradiation Facility at KUR [19]. The Temperature Controlled Irradiation Tube was used in this irradiation, which can control irradiation temperature with high accuracy by using electric heaters and two thermo-couples. The specimens were irradiated at 290 ± 2 °C in a low-pressure He atmosphere. The fast neutron flux was 9.4×10^{16} n/m^2/s in $E > 0.1$ MeV and 5.5×10^{16} n/m^2/s in $E > 1$ MeV. The neutron flux corresponded to the dpa rate of 8.8×10^{-9} dpa/s, calculated using neutron spectrum and ASTM E693 dpa cross sections of Fe. The final dpa was set at 1 and 10 mdpa.

The electron-irradiated samples used for the present PIA experiments were those already irradiated in the previous study [11]. The irradiation was conducted with 5 MeV electrons at 290 °C at the dpa rate of $1.7–2.0 \times 10^{-8}$ dpa/s to doses of 10–22 mdpa. The dose rate in KUR irradiation was very close to that in the electron irradiation. The dose range in KUR irradiation overlapped with that in the electron irradiation.

2.2. Measurements

Hardness, positron annihilation (PA) and three-dimensional atom probe (3DAP) measurements were applied to unirradiated, as-irradiated and post-irradiation annealed specimens.

Table 1
Chemical composition of steels (wt.%).

	C	Si	Mn	P	S	Ni	Cr	Mo	Cu	Fe
A	0.12	0.25	1.20	0.014	0.015	0.58	0.08	0.54	0.12	Balance
B	0.17	0.29	1.45	0.011	0.017	0.55	0.11	0.50	0.16	Balance
C	0.18	0.23	1.39	0.007	0.008	0.57	0.03	0.46	0.03	Balance

Vickers hardness was measured with a 500 g load. The hardness of each specimen was determined by averaging over 10 measurements. The coincident Doppler broadening (CDB) technique [20,21] and positron lifetime spectroscopy were performed on the disk shaped specimens. Details of the PA measurement methods were described in the previous paper [11]. 3DAP measurements were carried out using energy-compensated optical position-sensitive atom probe (ECOPoSAP) facilities [22] and a local electrode atom probe (LEAP [trademark of Imago Scientific Instruments Corporation]) facility [23]. The error originating from the evaporation aberration was less than 0.2 nm. The mass resolutions ($m/\Delta m$) were over 500 full widths at half maximum for ECOPoSAP and over 300 full widths at half maximum for LEAP. The rod shaped specimens were electropolished to form needles in a solution of 5% perchloric acid, glycerin and ethanol. Final electropolishing was performed using 2% perchloric acid in 2-butoxyethanol. Measurements were conducted at a sample temperature of 60 K with the pulse fraction of 0.15. In the present analysis, Ni-58, which is inseparable from Fe-58, was not used for evaluation of Ni.

In PIA experiments, isochronal annealing was applied at temperatures ranging from 250 to 650 °C at 50 °C intervals for 0.5 h. The PIA was applied to steels A and B irradiated to 10 mdpa in KUR, and steel A irradiated to 10 and 22 mdpa and steel B irradiated to 22 mdpa with 5 MeV electrons at 290 °C.

3. Results

3.1. As KUR-irradiated steels

Fig. 1 shows dose dependence of irradiation hardening (ΔHV) in steels A, B and C. The irradiation hardening increased with increasing dose and reached ~40 at 10 mdpa in steels A and B. Steel B showed slightly higher hardening than steel A due to its higher Cu concentration. The hardening of low Cu steel C was not significant at 10 mdpa within the data scatter band.

Fig. 2 shows CDB ratio curves for steels A, B and C, together with the curve for well-annealed pure Cu as a reference. The broad peaks around $P_L = 24 \times 10^{-3}\, m_0c$ are characteristic of Cu-3d electrons, indicating clustering of Cu atoms. The peak was observed in steels A and B after irradiation to 1 and 10 mdpa, and became clearer with higher dose. No peak was observed in steel C after irradiation to 10 mdpa. The ratios near $P_L = 0$ slightly increased with increasing dose up to 10 mdpa. The increase in the low-momentum region means an increase in the amount of open volume in the materials. Weak peaks at around $P_L = 24 \times 10^{-3}\, m_0c$ and $P_L = 0$ observed in unirradiated steels A and B in Fig. 2 suggested that pairs of vacancies and Cu atoms existed before the irradiation. Fig. 3 shows the dose dependence of S- and W-parameters, defined as the ratios of low-momentum ($|P_L| < 4 \times 10^{-3}\, m_0c$) and high-

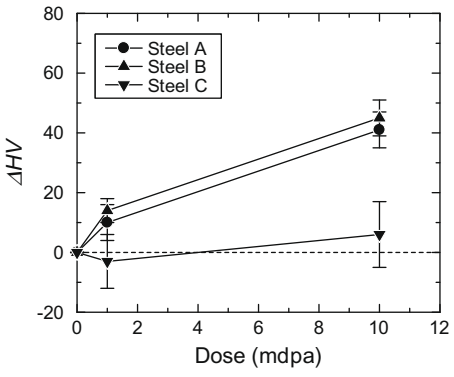

Fig. 1. Dose dependence of hardening (ΔHV) in steels A, B and C irradiated in KUR.

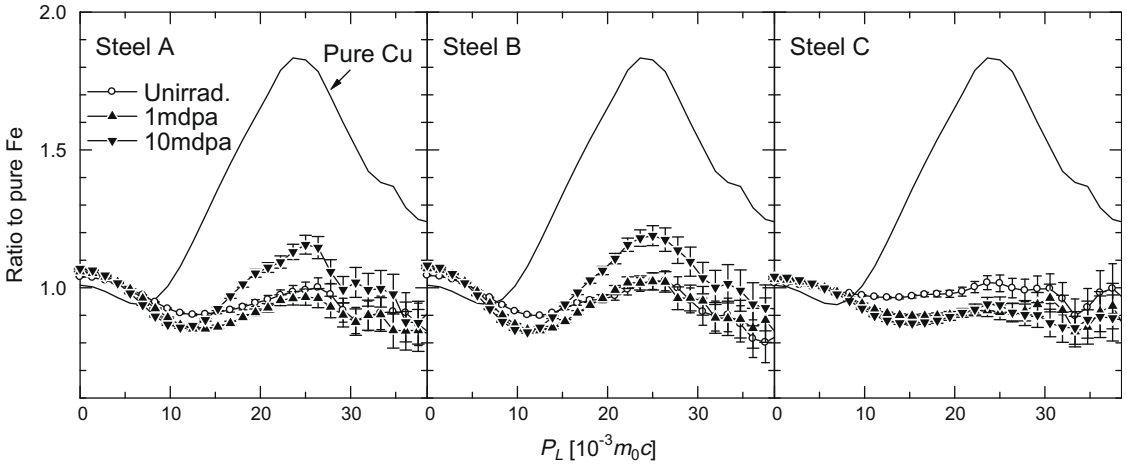

Fig. 2. CDB ratio curves for steels A, B and C irradiated in KUR.

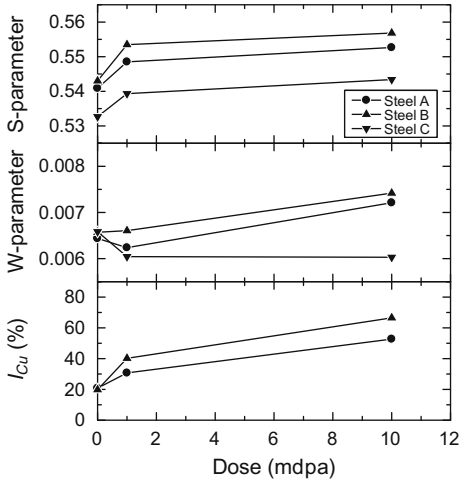

Fig. 3. Dose dependence of S-parameter, W-parameter and the fraction of the positron annihilation with Cu electrons (I_{Cu}) in steels A, B and C irradiated in KUR.

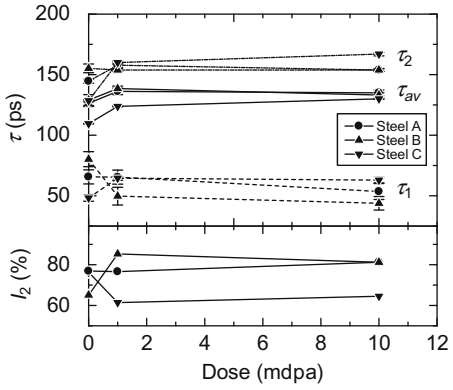

Fig. 4. Dose dependence of average positron lifetime (τ_{av}), shorter component (τ_1) and longer component (τ_2) and relative intensity of τ_2 component (I_2) irradiated in KUR.

momentum ($18 \times 10^{-3}\, m_0c < |P_L| < 30 \times 10^{-3}\, m_0c$) regions to the total region in the CDB ratio curves, respectively, and the fraction of the positron annihilation with Cu electrons (I_{Cu}) estimated from the height of the peak in the high-momentum region of the CDB ratio curves. Details of the definition of I_{Cu} were described in the previous paper [11]. I_{Cu} is shown only for steels A and B because no Cu peak was observed in steel C. The S-parameter clearly increased at 1 mdpa and saturated at 10 mdpa in all steels. The W-parameter in steels A and B showed a small change at 1 mdpa and then increased at 10 mdpa. In steel C, the W-parameter decreased at 1 mdpa and did not change with increasing dose. The increase in S-parameter means the increase in the amount of open volume in the matrix, and would result in the decrease of W-parameter. The open volume defects for the positron annihilation are assumed to be vacancies, vacancy-type defects and interstitial-type defects such as a dislocation loop. The increase in S-parameter in steels A, B and C at lower dose indicated that the accumulation of open volume defects occurred. The increase in W-parameter under the saturation of S-parameter means that the positron annihilation with Cu electrons becomes predominant. The increase in W-parameter in steels A and B at higher dose indicated that the positron annihilation with Cu electrons increased. I_{Cu} increased with increasing dose, reaching ~50% at 10 mdpa in steel A and ~70% at 10 mdpa in steel B. The W-parameter and I_{Cu} were higher for steel B, because Cu clustering was pronounced due to a higher Cu content in steel B. The CDB measurements indicated that the accumulation of open volume defects and Cu aggregation occurred in steels A and B and that only the accumulation of open volume defects occurred in steel C.

Fig. 4 shows the dose dependence of average positron lifetime (τ_{av}), shorter component (τ_1), longer component (τ_2), and relative intensity of τ_2 component (I_2). τ_{av} in all steels increased with increasing dose to 1 mdpa followed by saturation. τ_2 in the irradiated samples did not change to 10 mdpa and the value of τ_2 was ~160 ps, which was smaller than the lifetime of single vacancies in Fe (180 ps). Vacancy-type clusters such as microvoids were not formed under the present low dose neutron irradiation at 290 °C in all steels.

The detailed structure of solute clusters was obtained using 3DAP measurements. All steels irradiated to 10 mdpa were examined by using ECOPoSAP, which has higher mass resolution, to mainly obtain the detailed size and composition of clusters. Only steel B irradiated to 1 and 10 mdpa was also examined by using LEAP, which can measure a larger volume to mainly obtain the detailed number density of clusters. Fig. 5 show sets of three-dimensional atom maps in steel B irradiated to 10 mdpa by using LEAP. A large number of Cu clusters was observed in the Cu atom map. Mn, Ni and Si clustering were identified at the same region of Cu clusters. In this figure, one-dimensional P enriched regions were

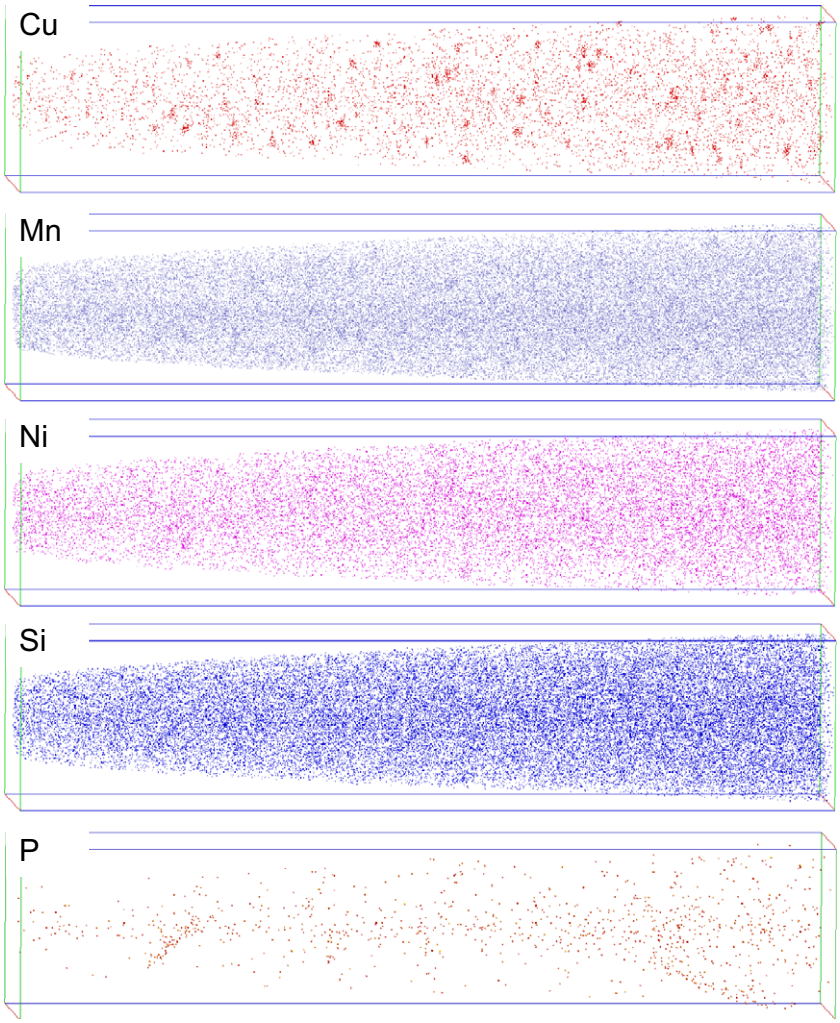

Fig. 5. 3D atom maps in 36 × 36 × 172 nm region in steel B irradiated to 10 mdpa in KUR.

observed together with enrichment of Si, which would show line dislocations. Fig. 6 shows enlarged atom maps for one Cu cluster in steel B irradiated to 10 mdpa by using ECOPoSAP. Aggregation of Cu atoms was clearly detected and accompanied by enrichment of Mn, Ni and Si atoms. This morphology was quite similar to those observed in the same steels irradiated to higher doses in a commercial reactor and material test reactor [24]. In low Cu steel C, no clustering of Cu, Mn, Ni, Si and P was identified in ECOPoSAP analyses. This indicated that clustering of solutes did not occur at doses as low as 10 mdpa in low Cu steels. No significant increase of the hardness in steel C after irradiation to 10 mdpa was likely consistent with the atom-probe observation.

The average diameter, number density and average composition of clusters are summarized in Table 2. In the present study, a solute cluster was defined as a cluster containing more than five Cu atoms with Cu–Cu distances of less than 0.7 nm. After determining a cluster, atoms belonging to the cluster were defined as those atoms that had at least four other Cu atoms within the distance of 1 nm. The radius of each Cu-rich cluster was determined as the radius of gyration for all atoms in the cluster. The difference in number density between ECOPoSAP and LEAP measurements was not large in spite of the large difference in measurement volume. For example, the number density determined by LEAP measurements in steel B irradiated to 1 and 10 mdpa was $1.1 \times 10^{23}/m^3$ (16 clusters in 150,000 nm^3) and $8.1 \times 10^{23}/m^3$ (86 clusters in 110,000 nm^3), respectively. The ECOPoSAP results were $2.4 \times 10^{23}/m^3$ (5 clusters in 21,000 nm^3) and $9.3 \times 10^{23}/m^3$ (32 clusters in 36,000 nm^3), respectively.

The average diameter was around 2 nm, and the number density was in the order of $10^{23}/m^3$. These values were very close to those reported in the same steels A and B irradiated to 50–100 mdpa at similar dose rates in a material test reactor (2.1 nm in diameter and $\sim 10 \times 10^{23}/m^3$ in number density) [24]. The average diameter and number density in steel B increased with dose from 1 to 10 mdpa and were larger than those in steel A at 10 mdpa. The higher Cu concentration in steel B (0.16%Cu) likely caused larger and more numerous Cu-rich clusters than in steel A (0.12%Cu). The composition of the clusters was Fe–(3–5)Cu–(1–3)Mn–(1–3)Ni–(1–2)Si, indicating that the clusters were very dilute.

3.2. PIA behavior

3.2.1. KUR-irradiated steels

PIA experiments were conducted on steels A and B irradiated to 10 mdpa in KUR. Fig. 7 shows the changes in hardness, W- and S-parameters, I_{Cu}, and positron lifetime (τ_{av}, τ_2 and I_2) during the annealing. The hardness recovery started at 400 °C, accelerated at 450–500 °C, and was almost complete at 600 °C. The W-parameter increased at 400 °C, reached a peak at 450 °C, and then decreased, whereas the S-parameter showed the opposite change. I_{Cu} showed a similar change to the W-parameter but decreased to a much

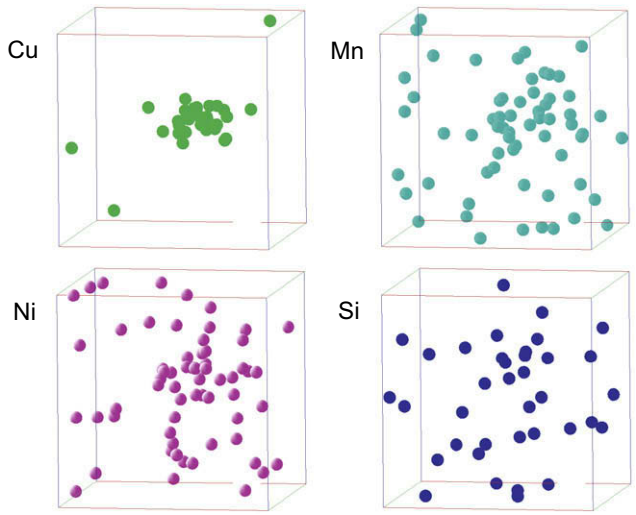

Fig. 6. Enlarged 3D atom maps (3 × 3 × 3 nm) showing a Cu cluster in steel B irradiated to 10 mdpa in KUR.

lower level than the as-irradiated level at 550–600 °C. These results indicated that Cu-rich clusters that could sufficiently capture positrons existed at temperatures below 450 °C, above which they disappeared gradually. The positron lifetimes showed similar changes in both steels A and B. τ_{av} and τ_2 started to decrease at 400 °C, reached a minimum at 450 °C and then increased at higher temperature. However, τ_2 did not exceed 180 ps, which corresponds to the positron lifetime of single vacancies in Fe (180 ps), suggesting that vacancy-type defects such as microvoids were not formed during annealing. I_2 did not change at temperatures below 450 °C, above which it decreased, whereas τ_2 showed a minimum at 450 °C. The results of PIA measurements indicated that the structure of positron-trapping sites such as Cu-rich clusters was altered at temperatures below 450 °C and that the density of positron-trapping sites decreased at temperatures above 500 °C.

Fig. 8 shows atom maps in steel B after annealing at 450 °C by using LEAP. A number of Cu clusters were detected. The average diameter, number density and average composition of clusters are summarized in Table 2. The average diameter and number density were 2.6 nm and $5.3 \times 10^{23}/m^3$, respectively. Compared to as-irradiated data, the number density decreased, likely showing thermal dissociation, whereas the average diameter showed no significant changes during the annealing. The annealing caused a decrease in Mn and Si fractions and an increase in Cu fraction in the clusters, whereas Ni fraction remained unchanged. This is more clearly confirmed in Fig. 9, which shows plots of concentration of Cu, Mn, Ni and Si versus diameter of a cluster before and after the annealing. The Cu concentration tended to increase in larger clusters. The concentrations of Mn and Si changed to the bulk concentration in half of the clusters and tended to decrease in smaller clusters. It is likely that Cu and Ni atoms were more tightly bound to clusters compared to Mn and Si atoms.

3.2.2. Electron-irradiated steels

PIA experiments were conducted on steel A irradiated to 10 and 22 mdpa and steel B irradiated to 22 mdpa with 5 MeV electrons. Fig. 10 shows the changes in hardness, W- and S-parameters, I_{Cu}, and positron lifetime (τ_{av}, τ_2 and I_2) during the annealing. The hardness recovery started at 400 °C in steel A and at 350 °C in steel B, accelerated at 400–450 °C, and was almost complete at 550 °C. The W-parameter increased at 400 °C, reached a peak at 450–500 °C, and then decreased, whereas the S-parameter showed the opposite change. I_{Cu} decreased at 500–550 °C. The positron lifetime of longer components (τ_2) showed a marked increase at 350 and 400 °C in steels irradiated to 22 mdpa. This temperature corresponded to the temperatures at which the hardening started to recover and the W-parameter increased. No substantial change in I_{Cu} at this temperature indicated that the substantial change did not occur at the capture site of positrons. These results indicated that the increase in the W-parameter at 400 °C was mainly related to the decrease in the S-parameter based on the diffusion and disappear of vacancies, and Cu clusters that could sufficiently capture positrons existed at temperatures below 500 °C, above which they disappeared gradually.

The positron lifetime of longer components (τ_2) showed an increase at 300 °C, and τ_2 exceeded 180 ps, which corresponds to the positron lifetime of single vacancies in Fe (180 ps), suggesting that vacancy-type defects such as microvoids were formed during the annealing. τ_2 showed a marked increase at 350 and 400 °C in steels irradiated to 22 mdpa but with small fraction of less than 10%, whereas the longer component could not be extracted at temperatures above 450 °C. This indicated that a small number of vacancy clusters containing 5–20 vacancies was formed at 400–450 °C and disappeared at higher temperatures. Such long-life components were not detected in steels A and B irradiated to 10 mdpa in KUR.

Fig. 11 shows 3D atom maps of Cu atoms and enlarged views of a Cu cluster in steel B irradiated with electrons after annealing at 350 and 450 °C by using ECOPoSAP. At 350 °C where the hardness started to recover without changes in S- and W-parameters, the as-irradiated morphology of clusters, namely a Cu core surrounded by Mn, Ni and Si, remained unchanged. However, at 450 °C where the hardness significantly recovered with a peak of W-parameter, clusters still remained but Cu aggregation seemed to be more loose and the surrounding Mn, Ni and Si atoms were lost. Although no quantitative data were obtained for these two annealed steels, the observed change in composition of the clusters due to annealing at 450 °C was consistent with that observed in KUR-irradiated steel B as mentioned above.

Table 2
Summary of clusters in steels irradiated in KUR at 290 °C.

Steel	Dose (mdpa)	Clusters						
		Diameter (nm)	Density ($10^{23}/m^3$)	Volume fraction	Composition (at.%)			
					Cu	Mn	Ni	Si
A	1	ND	ND	ND	ND	ND	ND	ND
	10	1.9	2.4	0.0009	5.1	2.8	2.8	0.8
B	1	2.1	1.1	0.0005	3.7	1.5	0.8	0.9
	10	2.5	8.1	0.0066	3.4	3.0	1.1	1.8
	10 + PIA	2.6	5.3	0.0048	4.1	1.6	0.9	1.0
C	10	ND	ND	ND	ND	ND	ND	ND

ND: not detected.
PIA: post-irradiation annealing at 450 °C for 30 min.

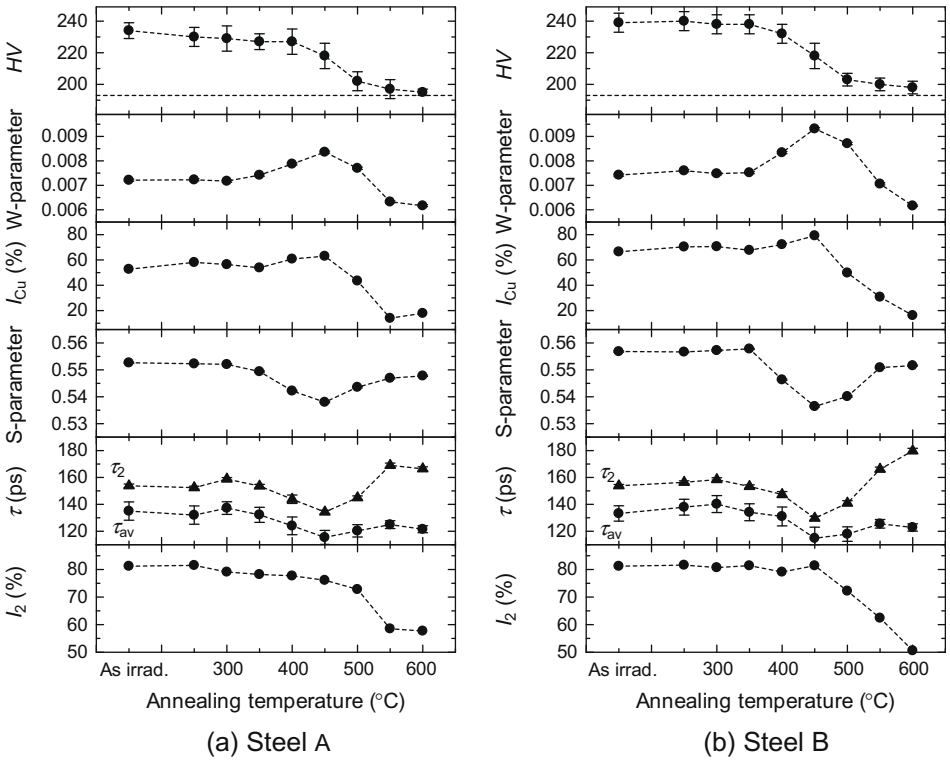

Fig. 7. Change in hardness, W- and S-parameter, I_{Cu} and positron lifetime during annealing in steels A and B irradiated to 10 mdpa in KUR.

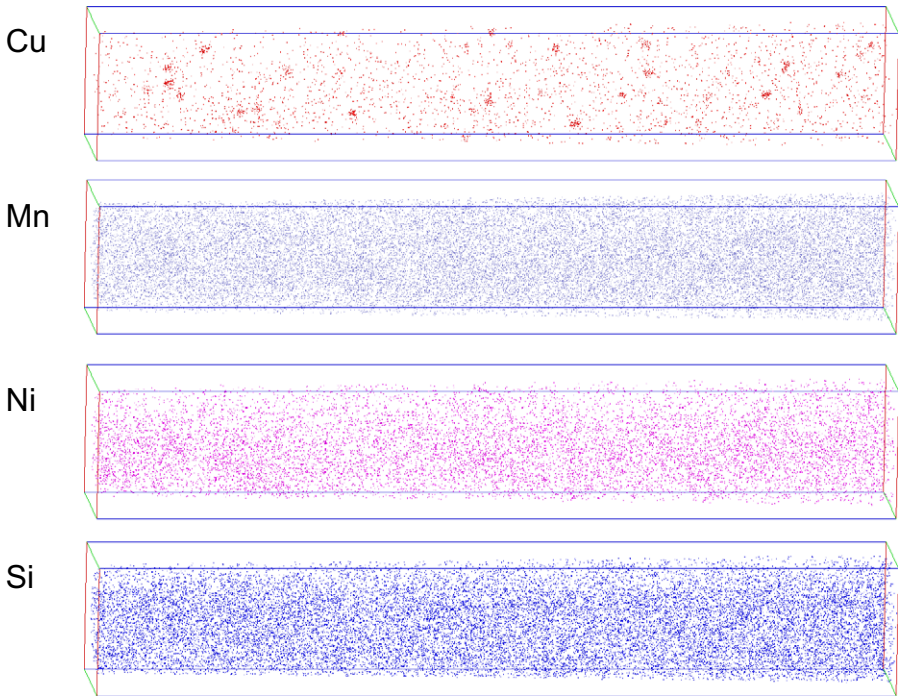

Fig. 8. 3D atom maps in 27 × 27 × 164 nm region in steel B irradiated to 10 mdpa in KUR after annealing at 450 °C.

4. Discussion

4.1. Evolution of solute clusters under low dose neutron irradiation

The combination of PA measurements and 3DAP analyses yielded detailed information on fine-scale microstructural evolution in the steels under low dose neutron irradiation at 290 °C. In medium Cu steels, Cu-rich clusters were readily formed at 1 mdpa and continuously formed up to 10 mdpa but the size slightly increased. The clusters were well defined with a number density in the order of $10^{23}/m^3$. The clusters were very dilute containing 3–5 at.%Cu, 1–3 at.%Mn, 1–3 at.%Ni and 1–2 at.%Si. Vacancies accumulated as mono vacancies at 1 mdpa but did not accumulate further up to 10 mdpa. In low Cu steel, no clusters were formed up to

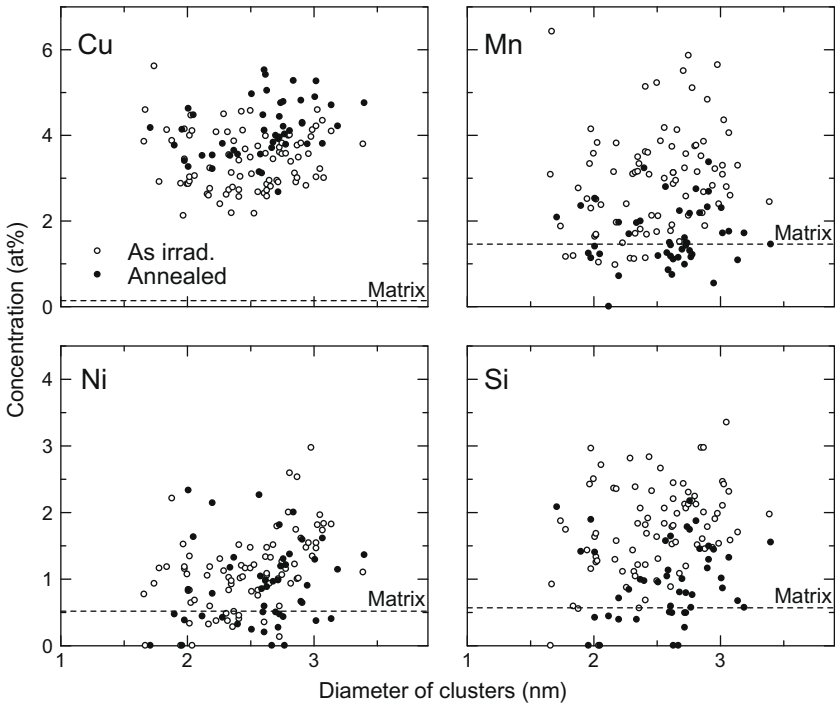

Fig. 9. Plots of concentration of Cu, Mn, Ni and Si versus diameter of a cluster in steel B irradiated to 10 mdpa in KUR before and after annealing at 450 °C. Matrix means chemical composition (at.%).

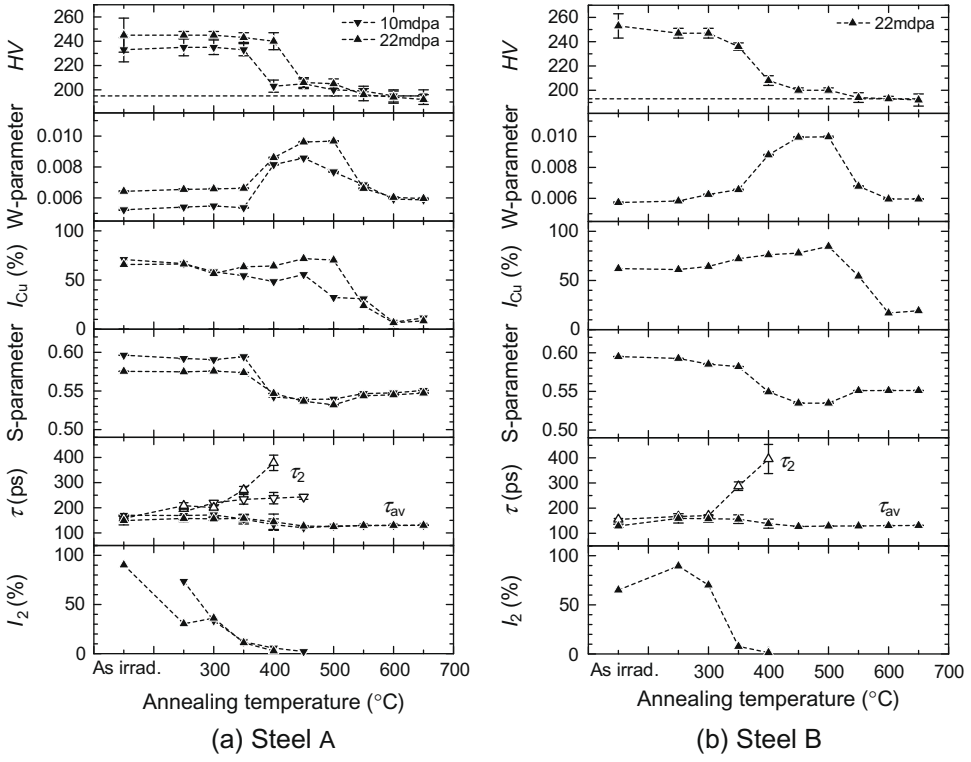

Fig. 10. Change in hardness, W- and S-parameter, I_{Cu}, and positron lifetime during annealing in steel A irradiated to 10 and 22 mdpa and steel B irradiated to 22 mdpa with 5 MeV electrons.

10 mdpa. The clusters were the main contributor to irradiation hardening.

PIA studies on medium Cu steels yielded information on the relation of Cu-rich clusters to hardening. The hardness in steels A and B irradiated to 10 mdpa showed rapid recovery at 450 °C and fully recovered at 600 °C. On the other hand, it was confirmed from the CBD measurements that the clustering of Cu atoms showed a maximum at 450 °C and disappeared at 600 °C. This indicated that Cu clusters that can capture positrons sufficiently existed at temperatures below 450 °C, above which they disappeared gradually.

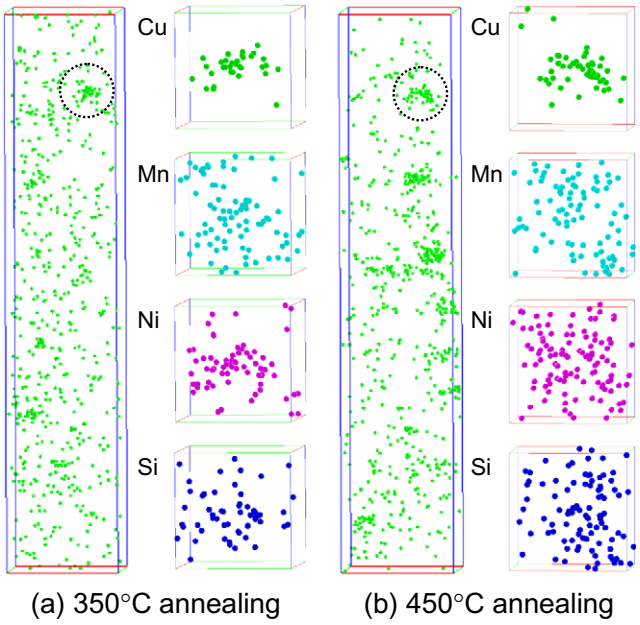

Fig. 11. Cu atom maps in $10 \times 10 \times 50$ nm region and enlarged 3D atom maps ($4 \times 4 \times 4$ nm) showing a Cu cluster in steel B irradiated to 22 mdpa with 5 MeV electrons after annealing at (a) 350 °C and (b) 450 °C.

The positron lifetime measurements revealed that the vacancy-type clusters such as microvoids were not formed during the annealing. Furthermore, it was also revealed that the structure of positron-trapping sites such as Cu-rich clusters changed at temperatures below 450 °C and that the density of positron-trapping sites decreased at temperatures above 500 °C. These observations indicated that a sufficiency of clusters existed to trap positrons after annealing at 450 °C whereas the irradiation hardening showed 50% recovery. The 3DAP observations for steel B after annealing at 450 °C provided clear evidence of the change of the clusters. The number density of the clusters decreased although the size remained unchanged after annealing as shown in Table 2. The volume fraction of the clusters decreased as a result of the decrease in the number density. This decrease in the volume fraction of 27% was smaller than the hardening recovery of ~50%. This difference is likely attributed to a change in hardening efficiency of the clusters due to a change in the composition of the clusters.

3DAP measurements revealed that the average Cu concentration in the clusters slightly increased after annealing at 450 °C as shown in Table 2. This was consistent with the increase in W-parameter in CDB measurements. The concentrations of Mn and Si obviously decreased after the annealing whereas Ni showed only a small change. Since the bulk chemical composition of steel B was Fe–0.1Cu–1.5Mn–0.5Ni–0.6Si in atomic fraction, the enrichment ratio of Mn in the clusters decreased from 2 to 1 by the annealing, whereas the enrichment ratio of Ni and Si after the annealing was about two. This can be rationalized by assuming the faster thermal dissociation of Mn atoms from the clusters than that of Ni and Si atoms. Although the compositional change of the clusters may be related to causing hardening recovery through weakened barrier strength for dislocation, the further experiments need for proof.

4.2. Comparison between electron and neutron irradiations

Hardening and cluster formation of the present medium Cu steels A and B were compared between KUR irradiation and 5 MeV electron irradiation, together with the previous high dose irradiation in a material test reactor (MTR) and a pressurized water reactor (PWR). Fig. 12 compares irradiation hardening (ΔHV) against dose. The trend line in Fig. 12 follows a power law expression, $\Delta HV \sim (\mathrm{dpa})^{1/3}$. At doses of 1–10 mdpa, the KUR irradiation data agreed well with the electron irradiation data. Higher dose neutron data lay on the trend line of the lower dose data within the data scatter band. These results indicated that neutron and electron irradiation at 290 °C causes almost the same irradiation hardening on a dpa basis at the dose rate of $\sim 1 \times 10^{-9}$ dpa/s.

Figs. 13 and 14 show comparisons of cluster data and composition between KUR and electron irradiation, respectively. The electron data in these figures were obtained by reanalyzing ECOPoSAP atom maps using the same cluster definition as the present KUR data. Both irradiations produced well-defined Cu-rich clusters, which had a Cu core surrounded by Mn, Ni and Si. The cluster morphology was basically the same as those reported in commercial steels irradiated with neutrons [24–26]. However, KUR irradiation produced slightly less numerous clusters with a slightly large diameter. The clusters produced under KUR irradiation contained larger amounts of solutes than those under electron irradiation, as seen in Fig. 14. This is more clearly confirmed in Fig. 15, which shows plots of the number of each solute versus the total numbers of solutes (Cu, Mn, Ni and Si) in a cluster for steel B irradiated to 10 mdpa in KUR and to 22 mdpa with electrons. The clusters in KUR-irradiated steel contained larger number of solute atoms than electron-irradiated steel in spite of a lower dpa for KUR irradiation. The present results confirmed that neutron irradiation produces well-defined clusters that are more solute-enriched with larger size and lower density compared to clusters produced by electron irradiation.

Regarding vacancy components evidenced by PA and PIA measurements, both electron and KUR irradiation did not produce microvoids. This was consistent with the reported results in commercial steels after neutron irradiation at 300 °C [27–29]. There are some notable differences between KUR and electron irradiation (Figs. 7 and 10). Electron irradiation showed a higher S-parameter in the as-irradiated condition, indicating that the amount of vacancies retained in the steel was higher for electron irradiation. Vacancy clusters, whether pure or solute-complex, were formed after annealing at 350–400 °C only in electron irradiation. A possible explanation for these data is that the clusters formed in electron irradiation contained more vacancies than those in KUR irradiation. Such clusters easily change properties by redistribution and dissociation of solute atoms and vacancies during annealing, as shown in Figs. 8, 9 and 11. This is likely responsible for lower temperature recovery of hardening in electron irradiation compared to KUR irradiation.

Fig. 16 shows a plot of hardening versus the square root of cluster volume fraction for all the present data. The hardening showed a linear dependence on the square root of cluster volume fraction.

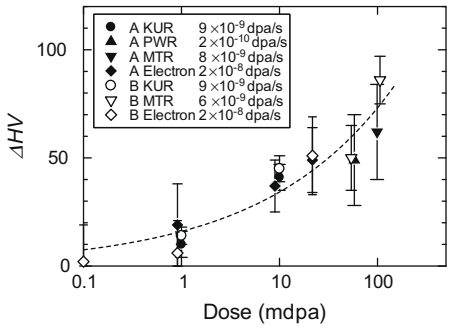

Fig. 12. Irradiation hardening in steels A and B under KUR irradiation together with the previous neutron and electron irradiation data.

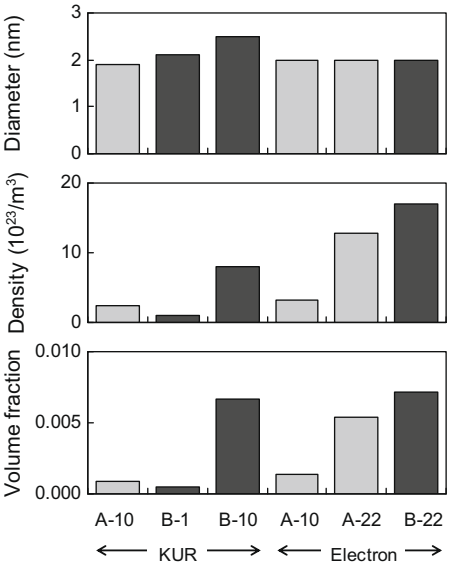

Fig. 13. Comparison of cluster data between KUR and electron irradiations. A-10 means steel A irradiated to 10 mdpa.

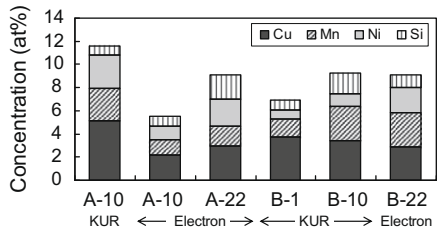

Fig. 14. Comparison of cluster composition between KUR and electron irradiations. A-10 means steel A irradiated to 10 mdpa.

This indicated that cluster formation dominated the hardening in both electron and neutron irradiations.

As a summary of the comparisons between KUR and electron irradiations for hardening and cluster formation in medium Cu steels under similar dose and dose rate conditions, both irradiations caused almost the same hardening on a dpa basis, dominated by Cu-rich clusters which were basically the same morphology. However, the KUR irradiation produced clusters that were more solute-enriched with larger size and lower density compared to clusters produced by electron irradiation. As discussed in the previous paper [11], these results likely indicated that cascade damage in neutron irradiation has an effect on Cu-rich cluster formation and resultant hardening since the surviving defects and freely-migrating vacancies under cascade damage are believed to be much lower in number than those under electron irradiation. To compensate the lower freely-migrating vacancy concentration for cluster formation, some enhancement effects should exist under cascade damage. Since Cu aggregation occurs via vacancy-driven diffusion of supersaturated Cu solutes, cascades likely enhance nucleation of Cu-rich clusters or provide direct nucleation sites through local high concentration of vacancies near each cascade. Cu and other solute atoms would be aggregated more effectively around cascade region due to locally high concentration of vacancies under neutron irradiation, compared to electron irradiation which provides uniformly distributed vacancies with a lower concentration in the matrix. This difference is considered to produce clusters that are more solute-enriched with larger size and lower density, in KUR irradiation. It is suggested that Cu-rich clusters are formed not only via radiation-enhanced diffusion but also via inhomogeneous radiation-induced nucleation under cascade damage. Further quantitative data and discussions are needed to clarify the cascade effects on the aggregation of Cu and other solute atoms.

5. Conclusion

Hardening and microstructure were examined in medium and low Cu A533B steels neutron-irradiated up to 10 mdpa in KUR by

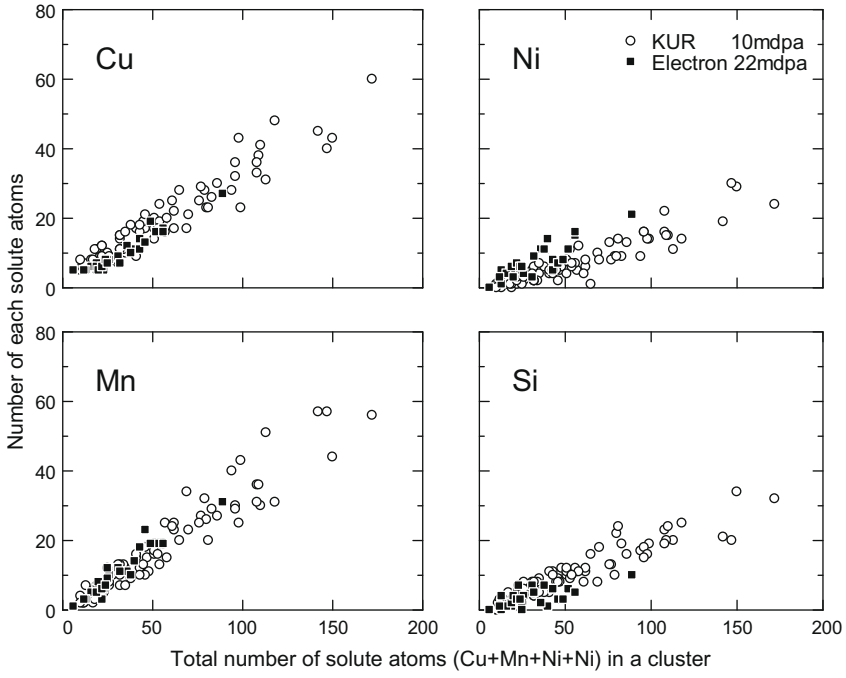

Fig. 15. Plots of number of Cu, Mn, Ni and Si atoms versus total number of solute atoms in a cluster in steel B irradiated to 10 mdpa in KUR and to 22 mdpa with 5 MeV electrons.

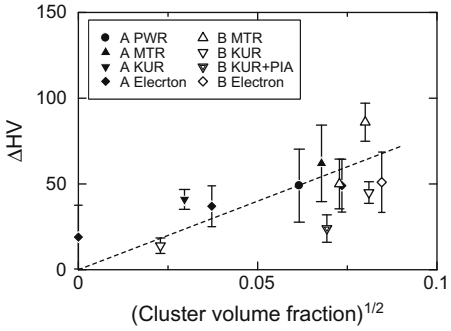

Fig. 16. Plot of hardening versus the square root of cluster volume fraction.

hardness, 3DAP and positron annihilation measurements. Post-irradiation annealing was applied to medium Cu steels irradiated in KUR and irradiated with 5 MeV electrons under almost the same dose and dose rate conditions.

In medium Cu steels, irradiation hardening increased with dose. Well-defined Cu-rich clusters were formed at doses as low as 1 mdpa, and the number density and size were increased at 10 mdpa. Both irradiation hardening and cluster formation showed dependence on Cu concentration. Neither hardening nor cluster formation was detected in low Cu steel. No microvoids were formed in any of the steels. Post-irradiation annealing in medium Cu steels revealed that the irradiation hardening started to recover at 350–400 °C and fully recovered at 600 °C. The Cu-rich clusters showed not only a decrease in number density but also compositional changes such as decrease in Mn and Si concentrations in the clusters during annealing. These changes could be attributed to hardness recovery.

Comparison of irradiation hardening and microstructure between neutron and electron irradiations in medium Cu steels revealed that neutron irradiation caused almost the same hardening and formed Cu-rich clusters, which were more solute-enriched but probably less vacancy-rich with larger size and lower density than those produced by electron irradiation. Considering the lower production of freely-migrating vacancies in neutron irradiation, the results suggested that cascades enhance the formation of Cu-rich clusters by providing a nucleation site for the clusters.

Acknowledgements

A part of this study was financially supported by the Budget for Nuclear Research of the Ministry of Education, Culture, Sports, Science and Technology, based on the screening and counseling by the Atomic Energy Commission.

References

[1] E. Eason, G.R. Odette, R.K. Nanstad, T. Yamamoto, ORNL/TM-2006/530, ORNL, February 2007.
[2] ASTM E 900-02, Guide for Predicting Radiation-Induced Transition Temperature Shift in Reactor Vessel Materials, E706 (IIF), Annual Book of ASTM Standards, vol. 12.02, ASTM, 2002.
[3] N. Hiranuma, N. Soneda, K. Dohi, S. Ishino, N. Dohi, H. Ohata, in: Proc. of 30th MPA-Seminar in Conjunction with the 9th German–Japanese Seminar, Stuttgart, October 2004.
[4] N. Soneda, K. Dohi, A. Nomoto, K. Nishida, S. Ishino, CRIEPI Q06019, CRIEPI, April 2007.
[5] G.R. Odette, G.E. Lucas, Radiat. Effects Defects Solids 144 (1998) 189–231.
[6] W.J. Phythian, C.A. English, J. Nucl. Mater. 205 (1993) 162–177.
[7] J.M. Hyde, D. Ellis, C.A. English, T.J. Williams, in: S.T. Rosinski et al. (Eds.), Effects of Radiation on Materials: 20th International Symposium, ASTM STP 1405, ASTM, 2001, pp. 262–288.
[8] M.K. Miller, R.K. Nastad, M.A. Sokolov, K.F. Russel, J. Nucl. Mater. 351 (2006) 187–196.
[9] K. Fujii, K. Fukuya, J. Nucl. Mater. 336 (2005) 323–330.
[10] N. Soneda, S. Ishino, A. Takahashi, K. Dohi, J. Nucl. Mater. 323 (2003) 169–180.
[11] K. Fujii, K. Fukuya, N. Nakata, K. Hono, Y. Nagai, M. Hasegawa, J. Nucl. Mater. 340 (2005) 247–258.
[12] D.E. Alexander, L.E. Rehn, K. Farrell, R.E. Stoller, J. Nucl. Mater. 228 (1996) 68–76.
[13] K. Farrell, R.E. Stoller, P. Jung, H. Ullmaier, J. Nucl. Mater. 279 (2000) 77–83.
[14] D.E. Alexander, L.E. Rehn, J. Nucl. Mater. 209 (1994) 212–214.
[15] R.E. Stoller, Nucl. Eng. Des. 195 (2000) 129–136.
[16] P. Auger, P. Pareige, S. Welzel, J.-C. Van Duysen, J. Nucl. Mater. 280 (2000) 331–344.
[17] P. Auger, P. Pareige, M. Akamatsu, J.-C. Van Duysen, J. Nucl. Mater. 211 (1994) 194–201.
[18] M.H. Mathon, A. Barbu, F. Dunstetter, F. Maury, N. Lorenzelli, C.H. de Novion, J. Nucl. Mater. 245 (1997) 224–237.
[19] T. Yoshiie, Y. Hayashi, S. Yanagita, Q. Xu, Y. Satoh, H. Tsujimoto, T. Kozuka, K. Kamae, K. Mishima, S. Shiroya, K. Kobayashi, M. Utsuro, Y. Fujita, Inst. Methods Phys. Res. A 498 (2003) 522–531.
[20] Y. Nagai, M. Hasegawa, Z. Tang, A. Hempel, K. Yubuta, T. Shimamura, Y. Kawazoe, A. Kawai, F. Kano, Phys. Rev. B 61 (2000) 6574.
[21] Y. Nagai, Z. Tang, M. Hasegawa, T. Kanai, M. Saneyasu, Phys. Rev. B 63 (2001) 134110.
[22] K. Hono, Acta Mater. 47 (1999) 3127–3145.
[23] T.F. Kelly, T.T. Gribb, J.D. Olson, R.L. Martens, J.D. Shepard, S.A. Wiener, T.C. Kunicki, R.M. Ulfig, D.R. Lenz, E.M. Strennen, E. Oltman, J.H. Bunton, D.R. Strait, Microsc. Microanal. 10 (2004) 373–383.
[24] K. Fukuya, K. Ohno, H. Nakata, S. Dumbill, J.M. Hyde, J. Nucl. Mater. 312 (2003) 163–173.
[25] T.J. Williams, D. Ellis, in: S.T. Rosinski et al. (Eds.), Effects of Radiation on Materials: 20th International Symposium, ASTM STP 1405, ASTM, 2001, pp. 8–27.
[26] R.G. Carter, N. Soneda, K. Dohi, J.M. Hyde, C.A. English, W.L. Server, J. Nucl. Mater. 298 (2001) 211–224.
[27] G. Brauer, L. Liszkay, B. Molnar, R. Krause, Nucl. Eng. Des. 127 (1991) 47–68.
[28] C. Lopes Gil, A.P. De Lima, N. Ayres De Campos, J.V. Fernandes, G. Kögel, P. Sperr, W. Triftshäuser, D. Pachur, Nucl. Mater. 161 (1989) 1–12.
[29] K. Ghazi-Wakili, U. Zimmermann, J. Brunner, P. Tipping, W.B. Waeber, F. Heinrich, Phys. Stat. Sol. (a) 102 (1987) 153–163.